

A MODEL FOR PREDICTING THE MICRO-SLIP ZONE ON A FRETTING CONTACT INTERFACE

**IRIMESCU Luminita¹, CIORNEI Florina Carmen¹, ALACI Stelian¹,
CERLINĂ Delia Aurora¹**

1. "Ștefan cel Mare" University of Suceava
luminita.irimescu@gmail.com

Keywords : micro-slip, fretting, interface stress state, surface failure

Abstract: The micro slip phenomenon is presents both in rolling and in sliding contacts. In the second case it appears in fretting contacts, were the main cause of failure is the surface degradation. This case was experimentally studied for a sphere-plane configuration, visualising where the micro-slips start. Then, the Huber-Mises-Hencky equivalent stress is numerically obtained in every contact point, by considering it to be responsible for surface failure. The theoretical results are in good agreement with the experimental analysis.

1. INTRODUCTION

The microslip phenomenon takes place in both rolling and sliding contacts. In the latter case it occurs in fretting, who is defined as a low amplitude oscillatory movement between bodies in mechanical contact. Such contact vibrations are often induced by vibration, cyclic load, cyclic accelerations, cyclic stresses, acoustic noises or thermal cycling.

The kinematics characteristics of movement yields to an interfacial micro-slip situation frequently encountered in industry due to machine vibrations. The characteristic of fretting is the contact area division in two parts: a stick zone and a micro-slip zone.

In this cases the surface degradation due to relative kinematics of contacting bodies is the main cause of products failure. The beginning of contact life, respectively the first relative movements of bodies are essential for the local destruction at interface.

Consequently, it's very important to understand the surface behaviour and the mechanism of micro-slip appearance. The approach uses the existent theoretical models and the concept of the velocity accommodation mechanism.

2. MODELS

The problem of partial sliding was first analysed by Cattaneo [1], and independently by Mindlin, [2]. They obtained a contact area divided into two zones, figure 1:

- a stick zone-a central elliptical zone, homotetics with the contact ellipse, where is no slip between contacting surfaces;
- a slip zone-an annulus zone where micro-slip occurs.

For spherical surfaces in contact, the equation for the energy dissipated per cycle in fretting was obtained by Mindlin and Deresiewicz, [3]:

$$\Delta W = \frac{9\mu^2 P_0^2}{10a} \left(\frac{2-\nu_1}{G_1} + \frac{2-\nu_2}{G_2} \right) \left\{ 1 - \left(1 - \frac{Q}{\mu P_0} \right)^{5/3} - \frac{Q}{6\mu P_0} \left[1 + \left(1 - \frac{Q}{\mu P_0} \right)^{2/3} \right] \right\}, \quad (1)$$

where - P_0 and Q are the normal and tangential load,

- a is the contact area radius,

- μ is the friction coefficient,

- $G_{1,2}$ and $\nu_{1,2}$ are shear moduli and corresponding Poisson's ratios.

Johnson, [4], find a reasonable agreement between the measured energy dissipation and that predicted by equation (1).

The Cattaneo-Mindlin model is an elastic model that considers the two contacting bodies perfectly elastic and perfectly smooth. In 1992, Odfalk and Vingsbo, [5], proposes an elastic-plastic model founded on the Cattaneo-Mindlin model, that considers the plastic deformations of the asperities.

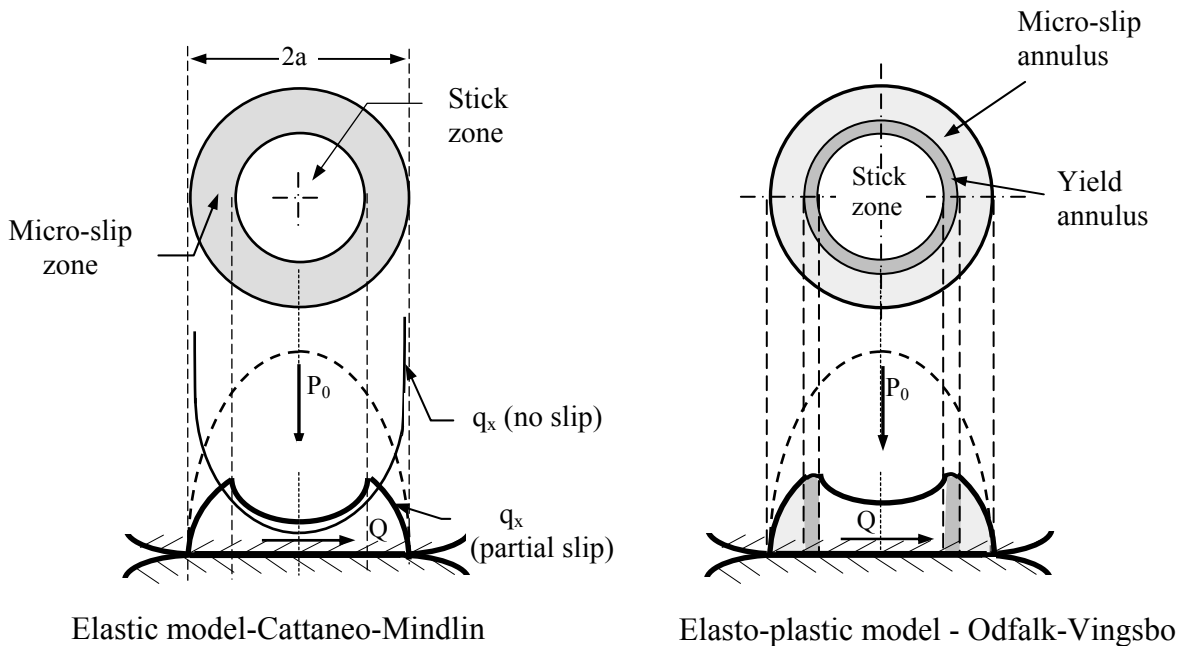


Figure 1: Theoretical models

The contact area is divided into three zones, figure 1:

- a central stick zone in which the asperities are elastically deformed;
- a peripheral slip annulus in which the asperities are sheared;
- an intermediate yield annulus in which the asperities are plastically deformed.

The transition of tangential traction between stick and micro-slip zone is no longer sharp but smooth.

2. CONCEPTS

Godet, [6], developed the interface tribology introducing the third-body model, which materialise the interface between two bodies in relative motion. This model gives a unified approach for all aspects of tribology, from thick film lubrication to dry friction. Godet, Berthier and their co-workers, [7],[8], introduced the concept of "velocity accommodation mechanism" for studying the friction and wear, summarised in figure 2.

According to this concept, a three-body contact can be divided into five basic elements known as sites S_1 to S_5 . This elements are: S_1, S_5 - the two solids in relative motion or first-bodies, S_3 - the interface or third-body bulk and S_2, S_4 - the two screens that separate that bulk from the third-body. The thickness of screens $S_{2,4}$ is only several nanometers, whereas that of site S_3 is usually of several micrometers.

The velocity accommodation can occur in anyone of the five sites according to four modes labelled as follow:

- M_1 – elastic;
- M_2 – rupture;

M_3 – shearing;
 M_4 – rolling.

The combination of five sites and four modes give rise to 20 velocity accommodation mechanisms labelled S_iM_j .

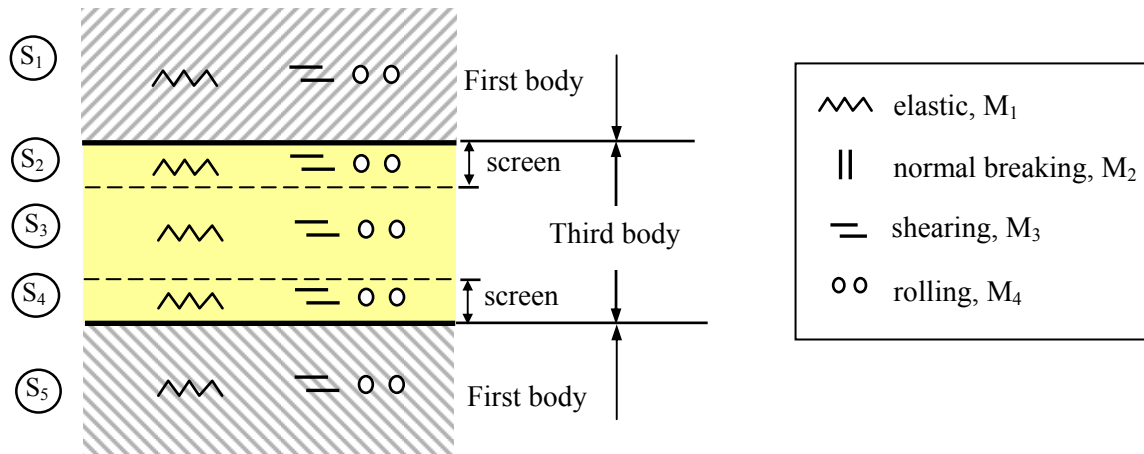


Figure 2: Velocity accommodation mechanism

3. TESTING EQUIPMENT

The experiments were performed using the testing machine "Tribomab" from the Mechanical Contact Laboratory, INSA Lyon, that simulates the fretting conditions, therefore a contact normally and tangentially loaded. The machine is illustrated schematically in figure 3.

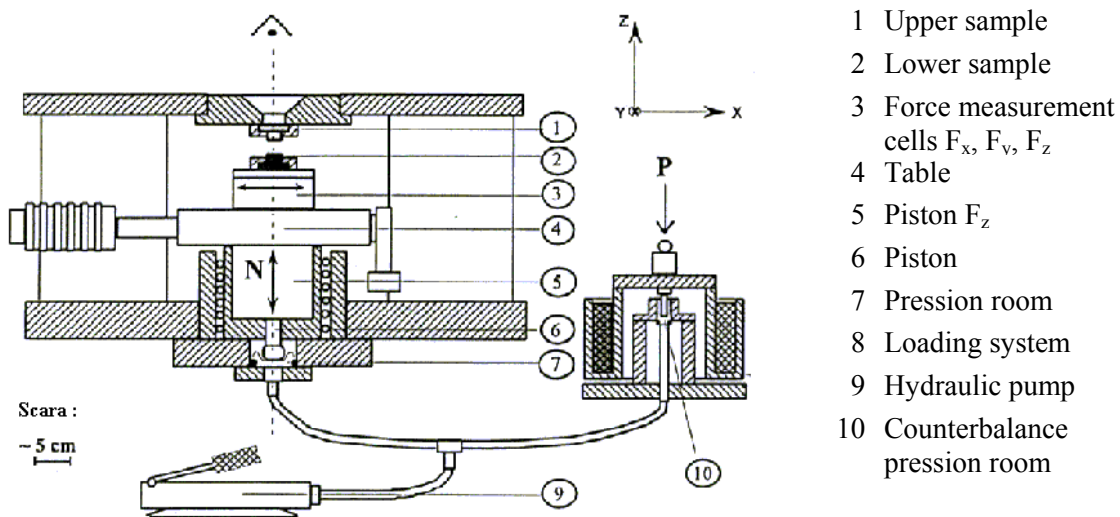


Figure 3: Testing machine TRIBOMAB

A computer controls the table (4) that gives the translation movement. The displacement on z direction is obtained with the hydraulic pump (9) and the gravitational loading system (8) that allow maintaining a constant normal load. The TRIBOMAB permit a movement on x direction with velocity between 0 to 4 mm/s. A video system can be install on the upper side of testing machine.

3. EXPERIMENTAL RESULTS

The contact used is of sphere-plane type. In order to analyse the microscopical evolution of the contact surface an artificial carbon screen obtained by vacuum sputter coating was used on the spherical steel sample. The thickness of carbon layer measured by laserprofilometry and illustrated in figure 4, is of few nanometers, [9], [10]. In order to allow the visualization and the filming of the contact interface, a transparent sample made of sapphire is used. The normal load is 180N and the movement amplitude increase from 10 μ m at the beginning to 40 μ m at the end of experiment.

The tribological life of the contact starts with the conception phase, when the two samples are bringing in contact and the first movements begin. Given the elastic dissimilarity between the two materials, when the normal load is applied, the sapphire tangential displacement of is half that of steel.

Consequently, there are some micro-slip and corresponding shear stresses even before the movement starts. The velocity difference is accommodated elastic and by shearing on the screen $S_{2,4}$ and the micro-slip annulus governed by the $S_{2,4}M_3$ mechanism begin to increase spreading toward the center of the contact area. In the presence of carbon screen, the friction is small enough for permitting the movement and avoiding the sample adherence.

After the local elimination of the screen, begin the direct interactions between the first bodies $S_{1,5}$ followed by an increasing of friction coefficient. Thus, the birth phase of the contact begins. Particles are detached from the first bodies by S_1M_2 and S_5M_2 mechanisms.

The third phase of the contact life is the proper life, when the third bodies is already formed and the velocity is accommodated almost completely elastically.

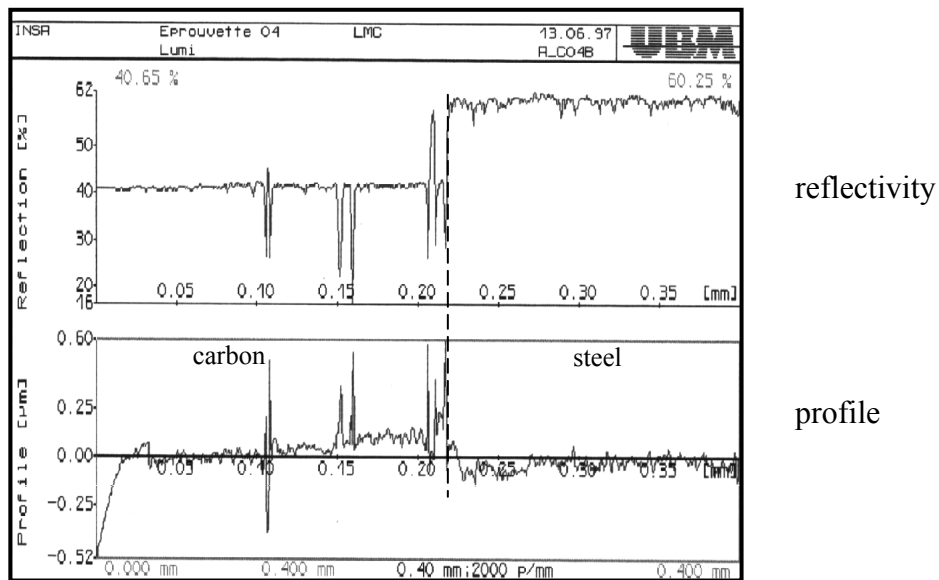


Figure 4: Carbon screen on the steel sample

The videotape that recorded the tests shows the appearance of micro-slip annulus after only a few cycles. The images acquisition from videotape and their analyze using a soft of image processing reveal first appearance of micro-slip traces on the edge of contact circle. Apparently, the first marks occur at the end of the diameter placed on the movement direction, figure 5.

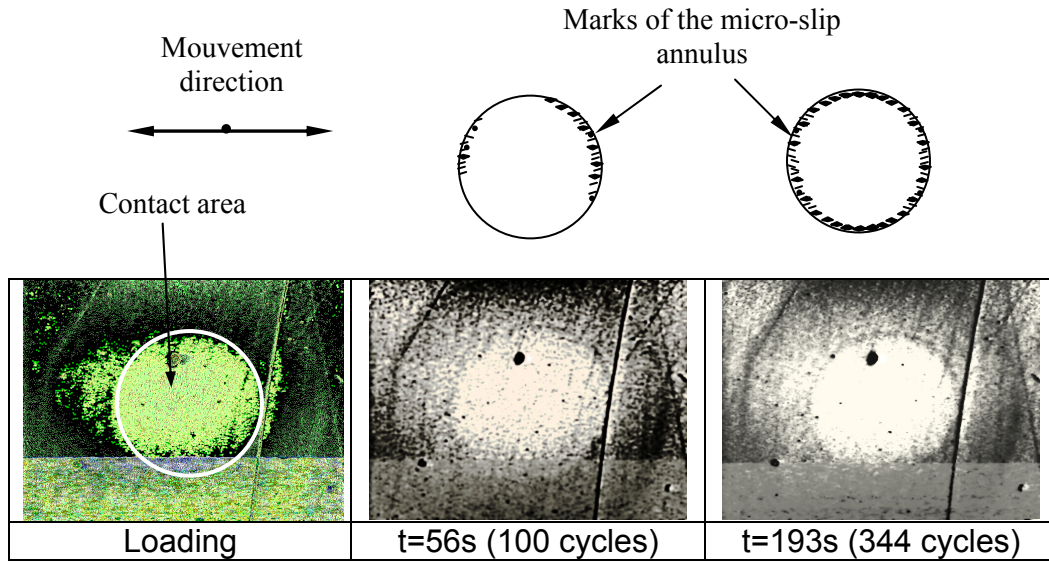


Figure 5: Images acquisition from the videotape

For explaining the experimental position of the first micro-slips, the global stress state on the contact interface due to normal and tangential loads was evaluated by adding the components due to normal and tangential load.. Hamilton and Goodman, [10], give the dimensionless stresses produced by a normal load in the points of circular contact area:

$$\begin{aligned} \bar{\sigma}_x &= \frac{(1-2\nu)}{3} \frac{(\bar{y}^2 - \bar{x}^2)}{\bar{\rho}^4} \left[(1-\bar{\rho}^2)^{\frac{3}{2}} - 1 \right] - \frac{1}{\bar{\rho}^2} (\bar{x}^2 - 2\nu\bar{y}^2) \sqrt{1-\bar{\rho}^2}; \\ \bar{\sigma}_y &= \frac{(1-2\nu)}{3} \frac{(\bar{x}^2 - \bar{y}^2)}{\bar{\rho}^4} \left[(1-\bar{\rho}^2)^{\frac{3}{2}} - 1 \right] - \frac{1}{\bar{\rho}^2} (\bar{y}^2 - 2\nu\bar{x}^2) \sqrt{1-\bar{\rho}^2}; \\ \bar{\sigma}_z &= -\sqrt{1-\bar{\rho}^2}; \quad \bar{\tau}_{xy} = \frac{(1-2\nu)}{3} \frac{\bar{x}\bar{y}}{\bar{\rho}^3} \left[2 - (2+\bar{\rho}^2) \sqrt{1-\bar{\rho}^2} \right]; \\ \bar{\tau}_{yz} &= \bar{\tau}_{zx} = 0. \end{aligned} \tag{2}$$

$$\bar{\rho}^2 = \bar{x}^2 + \bar{y}^2$$

where the dimensionless stresses $\bar{\sigma}_{ij} = \sigma_{ij} / p_0$ are expressed in terms of dimensionless coordinates $\bar{x} = x/a$, $\bar{y} = y/a$ and p_0 is the maximum Hertz pressure.

The contribution of tangential load on the global stress state was evaluated with the following relations, Hamilton and Goodman, [11]:

$$\begin{aligned} \bar{\sigma}_x &= -\frac{\pi}{8} (4 + \nu) \mu \bar{x}; \\ \bar{\sigma}_y &= -\frac{3\pi\nu}{8} \mu \bar{x}; \end{aligned} \tag{3}$$

$$\bar{\tau}_{xy} = -\frac{\pi}{8}(2-\nu)\mu\bar{y};$$

$$\bar{\tau}_{zx} = -\mu\sqrt{1-\rho^2}; \quad \bar{\sigma}_z = \bar{\tau}_{yz} = 0.$$

The global stresses generated in the points of contact area are numerically evaluated by aid of Mathcad soft and plotted as 3D and 2D graphs in terms of dimensionless coordinates X and Y, Figure 6. The calculation was made for the studied contact sphere (steel)-plane (sapphire), using the coefficient of friction measured during the first cycle of the test, $\mu=0,17$.

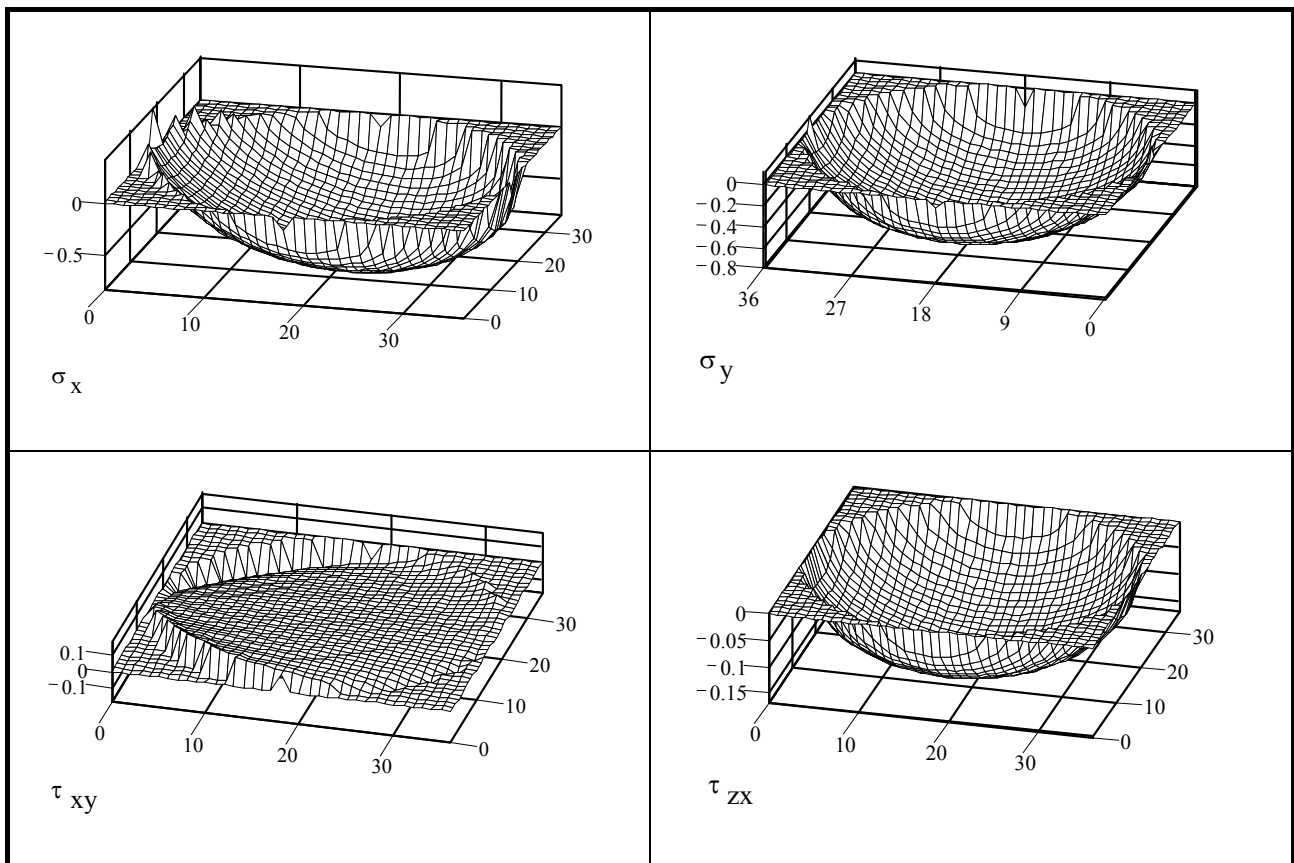


Figure 6: Stress state at the contact interface in fretting condition

The presence of relative movement induces a rise of normal stress σ_x that reach its maximum at the contact edge $x=-a, y=0$. This maximum value is $0,42 \cdot p_0$.

In order to taking into account the simultaneous action of all calculated stresses, an equivalent stress must be calculated. For the present situation, the Huber-Mises-Hencky is considered to be responsible for surface failure and consequently it is calculated in a dimensionless manner in every contact point by using the following equation:

$$\bar{\sigma}_E = \frac{1}{\sqrt{2}} \left[(\bar{\sigma}_x - \bar{\sigma}_y)^2 + (\bar{\sigma}_y - \sigma_z)^2 + (\bar{\sigma}_x - \bar{\sigma}_y)^2 + 6(\bar{\tau}_{xy}^2 + \bar{\tau}_{yz}^2 + \bar{\tau}_{zx}^2) \right]^{1/2} \quad (4)$$

The results for this equivalent stress are illustrated in Figures 7 a) and b) as a 3D graph and contour lines, respectively.

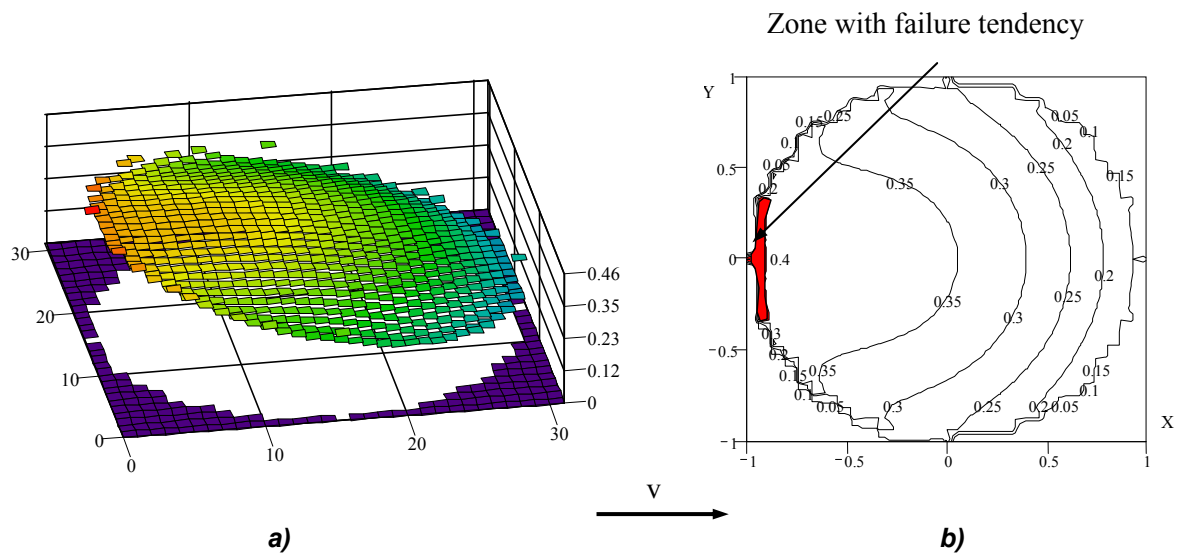


Figure 7: Huber-Mises-Hencky equivalent stress at the contact interface

The zone of maximum equivalent stress occurs at the back edge of the contact area in the point $(-a,0)$, where the Huber-Mises-Hencky equivalent stress has the value $0,46 \cdot p_0$ for a friction coefficient $\mu=0,17$. Consequently, the first zone subjected to deterioration is the trailing edge of the contact area, where the first micro-shearings of the carbon screen occur on the experiment.

4. CONCLUSION

The first experimental marks of screen micro-shearing were localised on the zones of maximum equivalent stress.

This proves the ability of Huber-Mises-Hencky stress to assess the occurrence of microslip at the interface of an elastic contact in fretting condition.

Consequently, the experiments permitted the validation of this equivalent stress for characterize the surface failure.

REFERENCES

- [1] Cattaneo, C.: Sul contatto di due corpi elastici: distribuzione locale degli sforzi, Rendiconti dell' Accademia nazionale dei Lincei, 27, Ser. 6, 1938, pp.342, 434, 474.
- [2] Mindlin, R. D.: Compliance of elastic bodies in contact, Trans. ASME, Series E, Journal of Applied Mechanics, 16, 1949, pp.259-268.
- [3] Mindlin, R.D. and Deresiewicz, H.: Elastic Spheres in contact under varying oblique forces, ASME J. of Appl. Mech., vol.20, 1953, pp. 327-344.
- [4] Johnson, K.L.: Surface interaction between elastically loaded bodies under tangential forces, Proc. R. Soc. London, Ser.A 230,1955, pp.531-548.
- [5] Odfalk, M. and Vingsbo, O.: An elastic - plastic model for fretting contact, Wear, 157, 1992, pp.435-444.
- [6] Godet, M.: The third-body approach: A mechanical view of wear, Wear, vol.100, 1984, pp.437-452.
- [7] Berthier Y., Brendle M., Godet M.: Velocity accommodation in friction, STLE, Tribology Transaction, vol. 32, n° 4, 1989, pp. 490-496.
- [8] Berthier, Y., 2001, Background on friction and wear, Lemaître Handbook of Materials Behaviour Models, Acad. Press, pp. 676-699.
- [9] Irimescu, L., Diaconescu, E.N., Berthier, Y.: La vie tribologique d'un contact, REFORT - Travaux scientifiques, ISBN 973-98210-9-X, Suceava, 1997, p.45-56.
- [10] Irimescu, L. Investigations upon relative kinematics and friction at an elastic contact interface, Ph. D Thesis, University of Suceava and INSA Lyon, 2002,.
- [11] Hamilton, G. M. & Goodman, L.E.: The stress field created by a circular sliding contact, ASME, J. of Appl. Mech., june,1966, pp.371-376.